AIAA Journal
Vol. 44, No. 7, July 2006

Inverse Evaluation of Material Constants for Piezoceramics by Out-of-Plane Vibration

Chi-Hung Huang*
Ching Yun University, Chung-Li 320, Taiwan, Republic of China

A full-field optical technique called amplitude-fluctuation electronic speckle pattern interferometry (AF-ESPI), together with out-of-plane measurement, is employed to investigate the vibration characteristics of completely free piezoceramic rectangular plates. Because the interferometric fringe patterns will be presented clearly only at resonant frequencies, both the resonant frequencies and the corresponding mode shapes are obtained by AF-ESPI at the same time. With the experimental results from the first few out-of-plane vibration modes, an inverse evaluation for the material compliance constants of piezoceramics is developed using the Rayleigh–Ritz method incorporated with the Simplex algorithm. As compared to the traditional method using radial in-plane modes of piezoceramic disks, the transverse resonant frequencies of rectangular plates are employed for the proposed methodology. Finite element method calculations are also performed to construct the mode shapes from the obtained material constants by inverse evaluation, and the results are compared with the experimental observations. This experimental method based on an optical AF-ESPI setup and the inverse algorithms proposed might become a reliable and self-consistent methodology for evaluating material constants of piezoceramic plates.

Nomenclature

A	=	amplitude of out-of-plane vibration
A'	=	amplitude of in-plane vibration
c^E_{ijkl}, c^E_{pq}	=	elastic constant at constant electrical field
D_i	=	electrical displacement component
D_{ij}	=	bending stiffness
d_{kp}	=	piezoelectric constant
E_k	=	electrical field component
e_{kij}, e_{kp}	=	piezoelectric constant
h	=	plate thickness
I_O	=	object light intensity
I_R	=	reference light intensity
J_0	=	zero-order Bessel function of first kind
J_1	=	first-order Bessel function of first kind
S_{ij}, S_p	=	strain component
s^E_{pq}	=	compliance constant at constant electrical field
T_{ij}, T_p	=	stress component
t	=	time
u_j	=	mechanical displacement field
x, y, z	=	Cartesian coordinate system
ε^S_{ik}	=	dielectric constant at constant strain
ε^T_{ik}	=	dielectric constant at constant stress
λ	=	wavelength of laser
ρ	=	material density
τ	=	charge-coupled device refreshing time
Φ	=	phase difference between reference and object lights
Φ'	=	phase difference between two object lights
Ψ	=	angle between object light and observation direction
Ψ'	=	one-half of angle between two object lights
ω	=	angular frequency

Introduction

BUTTERS and Leendertz[1] first proposed the basic principles of electronic speckle pattern interferometry (ESPI) for investigating the transverse vibration behavior of a disk. This technique (also called television holography or electronic holography) is a full-field, noncontact, and real-time method to measure the deformation of structures subjected to various kinds of loadings. As compared with traditional holographic interferometry,[2] the cumbersome and time-consuming chemical development can be omitted for ESPI, and the experimental process will be faster. Because only 1/30 s is needed to record and update a frame of interferometric pattern, ESPI is faster in operation and more insensitive to environmental disturbances than holography. However, this method cannot give as high an image quality as holographic interferometry due to the low resolution of the video camera system. However, for practical applications, these disadvantages are outweighed by the high sampling rate of the video camera. For these reasons, ESPI has become a powerful technique used for many academic studies and engineering applications. The most widely used experimental setup to study dynamic responses by ESPI is the time-averaged vibration measurement.[3] The disadvantage of this method is that the interferometric fringes represent the amplitude but not the phase of the vibration. To improve this shortcoming, the phase-modulation method using the reference beam modulation technique was developed to determine the relative phase of displacement.[4] Shellabear and Tyrer[5] used ESPI to make three-dimensional vibration measurements. Three different illumination geometries were constructed, and the orthogonal components of vibration amplitude and mode shape were determined. Løkberg[6] indicated that in-plane vibration modes could be obtained by using an out-of-plane setup and tilting the specimen with a proper angle. Doval et al.[7] proposed using additive stroboscopic television holography for out-of-plane vibration analysis, which exhibited enhanced contrast with constant visibility fringes and dynamic phase shifting. To reduce noise from the environment, the subtraction method was developed.[8] The subtraction method differs from the time-averaged method in that the reference frame is recorded before vibration and is continuously subtracted from the incoming frames after vibration. To both increase the visibility of the fringe pattern and reduce the environmental noise, an amplitude-fluctuation ESPI (AF-ESPI) method was proposed by Wang et al.[9] for out-of-plane vibration measurement. In the AF-ESPI method, the reference frame is recorded in a vibrating state and then subtracted from the incoming frame. Consequently, it combines the advantages of the time-averaged and subtraction methods, that is, good visibility and noise reduction. Ma and Huang[10] and Huang and Ma[11] used the AF-ESPI method to investigate the three-dimensional vibrations of piezoelectric rectangular parallelepipeds and cylinders, presenting and discussing in detail both the resonant frequencies and mode shapes.

Received 27 May 2004; revision received 8 August 2005; accepted for publication 29 January 2006.

*Associate Professor, Department of Mechanical Engineering; chhuang@cyu.edu.tw.

Piezoelectric transducers are widely used in electromechanical sensors, actuators, nondestructive testing devices, as well as electrooptic modulators, etc. The piezoelectric effect was discovered in 1880 by Pierre and Jacques Curie and had been addressed extensively in later literature.[12,13] The piezoelectric effect is applied to many modern engineering applications because it expresses the connection between the electrical and mechanical fields. Piezoelectricity describes the phenomenon that the material induces an electric charge when subjected to stress and, conversely, induces strain when the electric field is applied. Although the behavior of piezoelectric materials can be determined by linear electroelastic theory, the Maxwell equations, and piezoelectric constitutive equations,[14] analytical solutions can be obtained only for simple geometries. Previous studies[15,16] investigated the planar Poisson's ratio and electromechanical coupling factor for the piezoceramic materials. The IEEE Standard on Piezoelectricity[17] has been used to systematically present many formulations and equations that are based on the analysis of vibration in piezoelectric materials having simple geometric shapes. Beginning with the theory of piezoelectricity, many subjects, including the measurement of piezoelectric material constants, are presented in these standards. Chang et al.[18] formulated the electromechanical coupling coefficient (EMCC) for common piezoelectric ceramic elements and used numerical results to compare with methods proposed in other papers. Kosinski et al.[19] presented an improved resonator method to determine the piezoelectric material constants for a finite plate. This recommended measurement method, based on measurands unaffected by the vibration amplitude distribution, overcomes the one-dimensional approximation limitation in the IEEE Standard.

In this paper, an optical method based on the AF-ESPI is employed to study the vibration characteristics of piezoceramic rectangular plates with traction-free boundary conditions. The advantage of using the AF-ESPI method is that resonant frequencies and the corresponding mode shapes can be obtained simultaneously from the experimental measurement. By the use of the first few resonant frequencies of out-of-plane vibration for the piezoceramic rectangular plates, an inverse evaluation for the material constants is investigated. From the numerical analysis before the inverse evaluation, it is shown that the resonant frequencies of out-of-plane vibration modes are mainly dominated by the part of elastic (or compliance) constants. Consequently, the numbers of material constants for inverse evaluation are reduced, which agrees well with the experimental results. Moreover, finite element calculation is used to construct the mode shapes, and good agreements are obtained for both results. In comparison with the traditional method presented in the IEEE Standard, finite element calculation reveals that the inverse evaluation techniques applying the out-of-plane vibration modes might be an effective approach to determine material constants for piezoceramics.

Theory of Time-Averaged AF-ESPI Vibration Measurement

The optical arrangement of AF-ESPI for out-of-plane vibration measurement is shown schematically in Fig. 1. When the specimen vibrates periodically, the interferogram recorded by the charge-coupled device (CCD) camera is stored in an image buffer as a reference image. The light intensity of this reference image during the camera refreshing period can be expressed as

$$I_1 = \frac{1}{\tau}\int_0^\tau \left\{ I_O + I_R + 2\sqrt{I_O I_R} \times \cos\left[\Phi + \frac{2\pi A}{\lambda}(1+\cos\Psi)\cos\omega t\right]\right\} \mathrm{d}t \tag{1}$$

Let $\tau = 2m\pi/\omega$ and m be integers. Then, Eq. (1) can be solved as

$$I_1 = I_O + I_R + 2\sqrt{I_O I_R}(\cos\Phi)\cdot J_0[(2\pi A/\lambda)(1+\cos\Psi)] \tag{2}$$

After the image has been processed and rectified, the intensity of the reference (or first) image can be expressed as

$$I_1 = I_O + I_R + 2\sqrt{I_O I_R}|(\cos\Phi)\cdot J_0[(2\pi A/\lambda)(1+\cos\Psi)]| \tag{3}$$

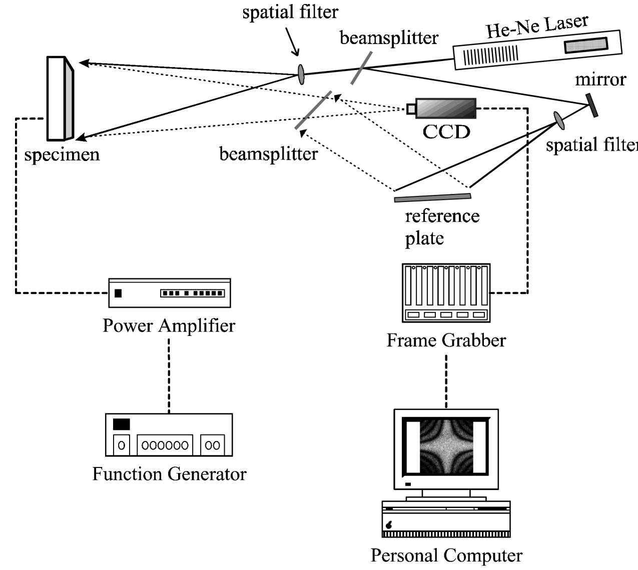

Fig. 1 Schematic of AF-ESPI setup for out-of-plane measurement.

As the vibration of the specimen continues, the vibration amplitude is assumed to change from A to $A + \Delta A$ because of the electronic noise or instability of the apparatus. According to Eq. (1), the light intensity of the second image can be represented as

$$I_2 = \frac{1}{\tau}\int_0^\tau \left\{ I_O + I_R + 2\sqrt{I_O I_R} \times \cos\left[\Phi + \frac{2\pi(A+\Delta A)}{\lambda}(1+\cos\Psi)\cos\omega t\right]\right\} \mathrm{d}t \tag{4}$$

When the vibration amplitude variation ΔA is rather small, Eq. (4) can be expanded in a Taylor series. By keeping the first two terms and neglecting the higher-order terms, we can rewrite Eq. (4) as follows:

$$I_2 = I_O + I_R + 2\sqrt{I_O I_R}(\cos\Phi)\left\{1 - \tfrac{1}{4}[(2\pi\Delta A/\lambda)(1+\cos\Psi)]^2\right\} \cdot J_0[(2\pi A/\lambda)(1+\cos\Psi)] \tag{5}$$

When the image is processed and rectified, I_2 can be similarly expressed as

$$I_2 = I_O + I_R + 2\sqrt{I_O I_R}\Big|(\cos\Phi)\left\{1 - \tfrac{1}{4}[(2\pi\Delta A/\lambda)(1+\cos\Psi)]^2\right\} \cdot J_0[(2\pi A/\lambda)(1+\cos\Psi)]\Big| \tag{6}$$

When these two images (the first and second images) are subtracted by the image processing system, that is, subtracting Eq. (3) from Eq. (6), and rectified, the resulting image intensity can be expressed as

$$I = I_2 - I_1 = \left(\sqrt{I_O I_R}/2\right)|(\cos\Phi)[(2\pi\Delta A/\lambda)(1+\cos\Psi)]^2 \cdot J_0[(2\pi A/\lambda)(1+\cos\Psi)]| \tag{7}$$

Equation (7) indicates that the fringe pattern for out-of-plane vibration obtained by the AF-ESPI method is controlled by the function J_0. The brightness lines of vibration interferometric patterns represent the nodal lines of mode shapes. This characteristic can be used as a qualitative observation or a quantitative analysis of the fringe patterns. Similar to the case of out-of-plane vibration, the resulting image intensity for the in-plane vibration measurement by the AF-ESPI method can also be derived as[10]

$$I = (I_O/2)\Big|(\cos\Phi')\cdot[(2\pi\Delta A'/\lambda)(2\sin\Psi')]^2 \cdot J_0[(2\pi A'/\lambda)(2\sin\Psi')]\Big| \tag{8}$$

Theory of Linear Piezoelectricity

For piezoelectric materials in nature, the mechanical deformation will be induced corresponding to the applied electrical field and vice versa. In other words, the equations of linear elasticity are coupled to the charge equation of electrostatics by means of the piezoelectric constants. The system of governing equations needed to determine the vibration characteristics of piezoelectric materials is presented as follows[14]: The differential equation of equilibrium is

$$T_{ij,i} = \rho \ddot{u}_j \tag{9}$$

The strain–mechanical displacement relations are

$$S_{ij} = \tfrac{1}{2}(u_{i,j} + u_{j,i}) \tag{10}$$

The charge equations of electrostatics are

$$D_{i,i} = 0 \tag{11}$$

The electric-field–electric-potential relations are

$$E_k = -\phi_{,k} \tag{12}$$

The linear piezoelectric constitutive equations are

$$T_{ij} = c^E_{ijkl} S_{kl} - e_{kij} E_k, \qquad D_i = e_{ikl} S_{kl} + \varepsilon^S_{ik} E_k \tag{13}$$

Because of symmetry, the compressed matrix (or engineering) notation is generally introduced in place of the tensor notation. The convention relating matrix and tensor notations consists of replacing ij or kl by p or q, where i, j, k, and l take the values 1–3 and p and q take the values 1, 2, 3, 4, 5, and 6. With the aid of this transformation, we can make the identifications

$$c^E_{ijkl} \equiv c^E_{pq}, \qquad e_{ikl} \equiv e_{iq}, \qquad T_{ij} \equiv T_p \tag{14}$$

and the constitutive equations (13) can be written as

$$T_p = c^E_{pq} S_q - e_{kp} E_k, \qquad D_i = e_{iq} S_q + \varepsilon^S_{ik} E_k \tag{15}$$

where

$$\begin{aligned} S_{kl} &= S_q \qquad \text{for} \qquad k = l, \qquad q = 1, 2, 3 \\ 2S_{kl} &= S_q \qquad \text{for} \qquad k \neq l, \qquad q = 4, 5, 6 \end{aligned}$$

The constitutive equations (15) have an alternative form expressed as

$$S_p = s^E_{pq} T_q + d_{kp} E_k, \qquad D_i = d_{iq} T_q + \varepsilon^T_{ik} E_k \tag{16}$$

Polarized piezoelectric ceramics have the symmetry of a hexagonal crystal in class $C_{6v} = 6$ mm that can be modeled as a transversely isotropic material. By Eq. (16), the linear piezoceramic constitutive equations can be represented in matrix form as

$$\begin{bmatrix} S_1 \\ S_2 \\ S_3 \\ S_4 \\ S_5 \\ S_6 \\ D_1 \\ D_2 \\ D_3 \end{bmatrix} = \begin{bmatrix} s^E_{11} & s^E_{12} & s^E_{13} & 0 & 0 & 0 & 0 & 0 & d_{31} \\ s^E_{12} & s^E_{11} & s^E_{13} & 0 & 0 & 0 & 0 & 0 & d_{31} \\ s^E_{13} & s^E_{13} & s^E_{33} & 0 & 0 & 0 & 0 & 0 & d_{33} \\ 0 & 0 & 0 & s^E_{44} & 0 & 0 & 0 & d_{15} & 0 \\ 0 & 0 & 0 & 0 & s^E_{44} & 0 & d_{15} & 0 & 0 \\ 0 & 0 & 0 & 0 & 0 & s^E_{66} & 0 & 0 & 0 \\ 0 & 0 & 0 & 0 & d_{15} & 0 & \varepsilon^T_{11} & 0 & 0 \\ 0 & 0 & 0 & d_{15} & 0 & 0 & 0 & \varepsilon^T_{11} & 0 \\ d_{31} & d_{31} & d_{33} & 0 & 0 & 0 & 0 & 0 & \varepsilon^T_{33} \end{bmatrix} \begin{bmatrix} T_1 \\ T_2 \\ T_3 \\ T_4 \\ T_5 \\ T_6 \\ E_1 \\ E_2 \\ E_3 \end{bmatrix} \tag{17}$$

Principle of Rayleigh–Ritz Method

The partial differential equation governing the out-of-plane motion of a thin orthotropic rectangular plate is

$$D_{11}\frac{\partial^4 w}{\partial x^4} + 2(D_{12} + D_{66})\frac{\partial^4 w}{\partial x^2 \partial y^2} + D_{22}\frac{\partial^4 w}{\partial y^4} = -\rho h \frac{\partial^2 w}{\partial t^2} \tag{18}$$

For free-harmonic vibrations at angular frequency ω, the out-of-plane displacement field can be assumed as

$$w(x, y, t) = W(x, y)\sin\omega t \tag{19}$$

where $W(x, y)$ is the maximum deflection function and can be represented as a linear series of assumed functions of the form

$$W(x, y) = \sum_{m=1}^{p}\sum_{n=1}^{q} A_{mn} X_m(x) Y_n(y) \tag{20}$$

The assumed functions $X_m(x)$ and $Y_n(y)$ must be admissible, such that they satisfy the essential boundary conditions of the plate. The characteristic equations of vibrating beams, termed beam functions, are used as the assumed functions $X_m(x)$ and $Y_n(y)$. The beam functions $X_m(x)$ and $Y_n(y)$ are chosen so that boundary conditions of the beams match those of the plate in the x and y directions, respectively; this will guarantee satisfaction of the essential boundary conditions for the rectangular plate. In this study, the free–free beam function is used as presented by Young.[20] When the stationary potential energy theory is used, the Rayleigh–Ritz method will provide a discrete number of stationary values that are the actual resonant frequencies of the plates.

Because the characteristics of piezoceramic plates is served as that for transverse isotropic plates, the relations between compliance and bending stiffness constants can be simplified and expressed as[21]

$$\begin{gathered} s^E_{11} = s^E_{22} = D_{11}\big/\left(D^2_{11} - D^2_{12}\right)\cdot h^3/12 \\ s^E_{12} = -D_{12}\big/\left(D^2_{11} - D^2_{12}\right)\cdot h^3/12, \qquad s^E_{66} = 1/D_{66}\cdot h^3/12 \end{gathered} \tag{21}$$

Hence, the inverse evaluation method developed for orthotropic plates can be applied to the investigation of piezoceramic plates.

Experimental Setup and Inverse Evaluation of Material Constants

The schematic layout of self-arranged time-averaged AF-ESPI optical systems, as shown in Fig. 1, are used to perform the out-of-plane experimental measurements for resonant frequencies and corresponding mode shapes. An He–Ne laser of 30 mW and a wavelength of $\lambda = 632.8$ nm is used as the coherent light source. The CCD camera (Pulnix Co.; TM-7CN) and frame grabber (Dipix Technologies, Inc.; P360F) with a digital signal processor onboard are used to record and process the images. As shown in Fig. 1 for the out-of-plane measurement, the laser beam is divided into two parts, the object and reference beams, by a beamsplitter. The object beam travels to the specimen and then reflects to the CCD camera. The reference beam is directed to the CCD camera via a mirror and a reference plate. The object and reference beams are combined into the CCD sensor array through a zoom lens. The CCD camera converts the intensity distribution, for the interference pattern of the object, into a corresponding video signal at 30 frames/ps. The signal is electronically processed and finally converted into an image on the video monitor. The interpretation of the fringe image is similar to a displacement contour map. To generate the sinusoidal excitation for the specimen, a digitally controlled function generator (Hewlett Packard; HP33120A) connected to a power amplifier (NF Electronic Instruments; Type 4005) is employed as an input source.

A piezoceramic rectangular plate made of $Pb(Zr \cdot Ti)O_3$ ceramics is selected for experimental investigations, and the model number

Table 1 Material properties of PIC-151 piezoceramics

Quantity	PIC-151
c_{11}^{E}, 10^{10} N/m^2	10.76
c_{33}^{E}, 10^{10} N/m^2	10.04
c_{12}^{E}, 10^{10} N/m^2	6.313
c_{13}^{E}, 10^{10} N/m^2	6.386
c_{44}^{E}, 10^{10} N/m^2	1.962
c_{66}^{E}, 10^{10} N/m^2	2.224
e_{31}, C/m^2	−9.522
e_{33}, C/m^2	15.14
e_{15}, C/m^2	11.97
ε_{11}^{S}, 10^{-9} F/m	9.832
ε_{33}^{S}, 10^{-9} F/m	8.185
ρ, kg/m^3	7800

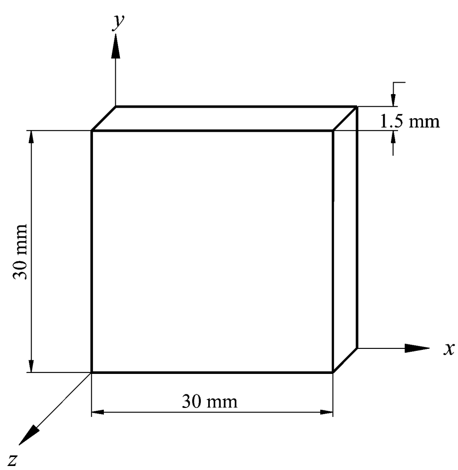

Fig. 2 Geometric dimensions of piezoceramic rectangular plate.

is PIC-151 (Physik Instrument Co.). The theoretical material constants provided by the manufacturer and geometric dimensions of the specimen are shown in Table 1 and Fig. 2, respectively. The polarization is along the z direction, and two opposite surfaces (x–y plane) of the specimen are completely coated with silver electrodes. The specimen is supported on a soft sponge to simulate the traction-free boundary conditions for theoretical and experimental investigations. The resonant frequencies and the corresponding mode shapes for the piezoceramic rectangular plate are determined experimentally by the optical method of AF-ESPI. The first few resonant frequencies determined experimentally are employed for inverse evaluation of the material constants of the tested plate. This inverse evaluation methodology, by the Rayleigh–Ritz method and the Simplex algorithm, has been employed for the composite plate and discussed in detail by Ma and Lin.[22] By means of Eq. (21), the inverse evaluation method for orthotropic plates can be applied to the piezoceramic rectangular plates. Here, an error function is introduced to quantify the difference between the inverse value and experimental result:

$$E = \sum_{i=1}^{N} \left(\frac{\omega_i - \omega_i^{\exp}}{\omega_i^{\exp}} \right)^2 \tag{22}$$

where N is the total number of the resonant frequencies to be used for inverse evaluation, ω_i is the reconstructed resonant frequency obtained from the inverse value of material constants, and $\omega_i^{\exp}$ is the experimental result of resonant frequencies by AF-ESPI. The material constants optimally searched must be such that the error function E is the global minimum value. The convergence criterion used for the Simplex algorithm is that the difference of the material constants obtained between the two iterations is less than 0.01%. In addition to experimental measurement, numerical calculation is also performed by the commercially available software ABAQUS finite element package,[23] from which 20-node three-dimensional quadratic brick element (C3D20E) and $10 \times 10 \times 1$ finite element meshes are selected to carry out the free-vibration analysis. The electrical potential between the two opposite surfaces is specified as zero to simulate the closed-circuit condition and extract the resonant frequency.

Because the piezoceramic constitution includes 10 independent material constants, as shown in Eq. (17), the influence of these material constants on the out-of-plane vibration modes must initially be investigated. Table 2 shows the results for the first five resonant frequencies according to the variations of individual independent material constants. The resonant frequencies of the piezoceramic rectangular plate shown in Table 2 are calculated by the finite element method (FEM) according to the theoretical material constants shown in Table 1. Because of the input formats for ABAQUS, the constitutive equations in Eq. (15) are adopted, and the constants c_{ij}^{E}, e_{ij}, and ε_{ij}^{S} are chosen to perform the finite element analysis. The results in Table 2 show that the resonant frequencies remain almost constant except for the variations of elastic constants c_{11}^{E} and c_{12}^{E}. It is known that the elastic constant matrix c_{ij}^{E} is the inverse of the compliance constant matrix s_{ij}^{E}. Consequently, the inverse evaluation will concentrate on the compliance constants in this study. Because the construction of the inverse evaluation is based on the vibration theory of orthotropic plates, it is necessary to compare those with piezoceramic plates. The parentheses in Table 2 represent the resonant frequencies calculated by the FEM, which are based on the assumption of orthotropic plates, and only the elastic constants c_{ij}^{E} are discussed. When these two results are compared in Table 2, the resonant frequency difference of the third mode is more than 20%, which will result in excluding the third mode in the inverse evaluation procedure. Five different initial guesses, as shown in Table 3, with different material compliance constant combinations are performed for the inverse calculations. These initial guess values are used to determine the resonant frequencies by a computer program in which equations are derived from the Rayleigh–Ritz method. When the Simplex algorithms are used, the iteration procedure is performed until convergence values of the material constants are obtained. The five different initial guesses converge to almost the same results, as indicated in Table 3, which shows the good convergence characteristics for the Simplex algorithms. The iteration numbers are from 139 to 293, which depend on the value of the initial guess and the convergence criterion. The difference between the inverse and theoretical values is mainly due to the errors induced by measuring the resonant frequencies from the AF-ESPI technique and the accuracy of the Rayleigh–Ritz method. It is shown that the inverse values in parentheses in Table 3 are determined according to resonant frequencies calculated by the FEM, which refers to the theoretical material constants. The difference between the inverse values calculated by the FEM and theoretical values is also presented in parentheses in Table 3; the results imply the suitability of the Rayleigh–Ritz method for piezoceramic rectangular plates to some extent when compared with the numerical analysis. The iteration and convergence of the material compliance constants for the fifth initial guess are shown in Fig. 3. The resonant frequencies obtained by the AF-ESPI measurement, the FEM, and the Rayleigh–Ritz method are shown in Table 4; both the FEM and Rayleigh–Ritz method calculations are performed with the inverse evaluated constants identified using the proposed method. Note that the inverse estimated resonant frequencies by the Rayleigh–Ritz method agree very well with the experimental results. This also demonstrates the excellent reliability and convergence of the Simplex algorithms for inverse evaluations of the material constants by using resonant frequencies of the out-of-plane vibration modes.

From the obtained inverse evaluation of the material compliance constants, the first five mode shapes are computed using ABAQUS, and the results are compared with the experimental observation from AF-ESPI, as shown in Fig. 4. We indicate the phase of displacement in the finite element results by a solid or dashed line, with the solid lines laying in the direction opposite the dashed lines. The transition

Table 2 Relations between the first five resonant frequencies and variations of individual material constants (values in hertz)

Out-of-plane mode	+10%	+5%	0	−5%	−10%
			Variation c_{11}^E		
1	3,232 (3,205)	3,078 (3,052)	2,915 (2,890)	2,741 (2,717)	2,553 (2,531)
2	4,882 (4,724)	4,657 (4,504)	4,418 (4,272)	4,163 (4,024)	3,887 (3,758)
3	7,177 (5,796)	7,013 (5,618)	6,839 (5,433)	6,652 (5,239)	6,447 (5,034)
4	8,609 (8,201)	8,239 (7,844)	7,844 (7,465)	7,419 (7,059)	6,956 (6,621)
5	15,788 (14,755)	15,189 (14,139)	14,556 (13,488)	13,881 (12,791)	13,159 (12,041)
			Variation c_{12}^E		
1	2,711 (2,692)	2,815 (2,793)	2,915 (2,890)	3,010 (2,982)	3,102 (3,071)
2	4,131 (4,014)	4,278 (4,147)	4,418 (4,272)	4,551 (4,390)	4,678 (4,500)
3	6,812 (5,509)	6,831 (5,475)	6,839 (5,433)	6,839 (5,385)	6,831 (5,332)
4	7,378 (7,075)	7,618 (7,278)	7,844 (7,465)	8,056 (7,637)	8,256 (7,795)
5	13,920 (12,883)	14,244 (13,194)	14,556 (13,488)	14,854 (13,762)	15,141 (14,020)
			Variation c_{13}^E		
1	2,913 (2,879)	2,914 (2,885)	2,915 (2,890)	2,916 (2,894)	2,917 (2,898)
2	4,405 (4,212)	4,412 (4,245)	4,418 (4,272)	4,424 (4,295)	4,429 (4,315)
3	6,677 (4,982)	6,762 (5,221)	6,839 (5,433)	6,910 (5,623)	6,974 (5,794)
4	7,810 (7,308)	7,828 (7,394)	7,844 (7,465)	7,859 (7,525)	7,872 (7,576)
5	14,435 (13,162)	14,498 (13,336)	14,556 (13,488)	14,610 (13,623)	14,659 (13,744)
			Variation c_{33}^E		
1	2,916 (2,894)	2,915 (2,892)	2,915 (2,890)	2,915 (2,888)	2,914 (2,885)
2	4,421 (4,293)	4,420 (4,284)	4,418 (4,272)	4,416 (4,258)	4,414 (4,242)
3	6,878 (5,611)	6,859 (5,527)	6,839 (5,433)	6,818 (5,326)	6,794 (5,202)
4	7,852 (7,521)	7,849 (7,495)	7,844 (7,465)	7,840 (7,430)	7,835 (7,388)
5	14,585 (13,614)	14,571 (13,555)	14,556 (13,488)	14,540 (13,411)	14,522 (13,322)
			Variation c_{44}^E		
1	2,919 (2,894)	2,917 (2,892)	2,915 (2,890)	2,913 (2,888)	2,910 (2,886)
2	4,419 (4,274)	4,419 (4,273)	4,418 (4,272)	4,417 (4,271)	4,417 (4,270)
3	6,845 (5,436)	6,842 (5,435)	6,839 (5,433)	6,836 (5,431)	6,833 (5,429)
4	7,858 (7,478)	7,851 (7,472)	7,844 (7,465)	7,837 (7,458)	7,829 (7,451)
5	14,593 (13,523)	14,575 (13,506)	14,556 (13,488)	14,535 (13,468)	14,513 (13,446)
			Variation e_{15}		
1	2,915	2,915	2,915	2,915	2,915
2	4,419	4,418	4,418	4,418	4,418
3	6,841	6,840	6,839	6,839	6,838
4	7,846	7,845	7,844	7,844	7,843
5	14,563	14,559	14,556	14,553	14,549
			Variation e_{31}		
1	2,914	2,914	2,915	2,916	2,916
2	4,409	4,413	4,418	4,423	4,427
3	6,727	6,783	6,839	6,896	6,953
4	7,820	7,833	7,844	7,856	7,868
5	14,469	14,512	14,556	14,600	14,645
			Variation e_{33}		
1	2,916	2,915	2,915	2,915	2,914
2	4,423	4,421	4,418	4,415	4,412
3	6,901	6,871	6,839	6,806	6,772
4	7,857	7,851	7,844	7,838	7,830
5	14,603	14,580	14,556	14,531	14,504
			Variation ε_{11}^S		
1	2,915	2,915	2,915	2,915	2,915
2	4,418	4,418	4,418	4,418	4,418
3	6,839	6,839	6,839	6,840	6,840
4	7,844	7,844	7,844	7,845	7,845
5	14,555	14,555	14,556	14,557	14,557
			Variation ε_{33}^S		
1	2,914	2,914	2,915	2,916	2,916
2	4,411	4,414	4,418	4,422	4,426
3	6,755	6,796	6,839	6,885	6,935
4	7,826	7,835	7,844	7,854	7,865
5	14,490	14,522	14,556	14,593	14,632

from solid lines to dashed lines corresponds to a zero displacement line, or a nodal line. The zero-order fringe, which is the brightest fringe in the experimental results, represents the nodal lines of the vibrating piezoceramic rectangular plate at resonant frequencies. The other fringes represent contours of constant amplitudes of the out-of-plane displacement. Note that the mode shapes obtained experimentally are in good agreement with those obtained numerically. Also note that, if there are resonant frequencies that are either missing or are not in order in the experimental measurement, then large errors will be induced in evaluating the material constants. However, because the resonant frequency and mode shape are obtained experimentally at the same time, the resonant frequency can be used exactly for the inverse evaluation of the material constants. The corresponding mode shape can served as a verification of the results to ensure that no missing or mismatch of the resonant frequency will occur.

Table 3 Inverse evaluations of material compliance constants for five different initial guesses and iteration number

	s_{11}^E, $10^{-12}\mathrm{m}^2/\mathrm{N}$		s_{22}^E, $10^{-12}\mathrm{m}^2/\mathrm{N}$		s_{12}^E, $10^{-12}\mathrm{m}^2/\mathrm{N}$		s_{66}^E, $10^{-12}\mathrm{m}^2/\mathrm{N}$		
Initial guess number	Initial guess	Converge value	Initial guess	Converge value	Initial guess	Converge value	Initial guess	Converge value	Iteration number
1	5	15.781	5	15.781	−2	−6.214	30	44.821	261
2	15	15.782	15	15.782	−10	−6.213	40	44.821	181
3	25	15.772	25	15.772	−20	−6.202	80	44.835	139
4	40	15.778	60	15.778	−15	−6.216	20	44.835	293
5	75	15.779	55	15.779	−55	−6.210	50	44.821	184
Theoretical value	16.83 (16.198)[a]		16.83 (16.198)		−5.656(−6.200)		44.97 (44.790)		
Difference, %	6.2 (3.8)		6.2 (3.8)		9.8 (9.6)		0.3 (0.4)		

[a]Values in parentheses represent inverse values obtained by FEM with theoretical material constants.

Table 4 Resonant frequencies obtained by AF-ESPI, FEM, and Rayleigh–Ritz method

Out-of-plane mode	Rayleigh–Ritz method, method A, Hz	AF-ESPI, method B, Hz	FEM, method C, Hz	Difference, method A/B, %	Difference, method A/C, %
1	2,969	2,970	2,915	−0.03	1.85
2	4,476	4,480	4,418	−0.09	1.31
3	——	6,770	6,839	——	——
4	7,912	7,880	7,844	0.41	0.87
5	14,538	14,580	14,556	−0.29	−0.12

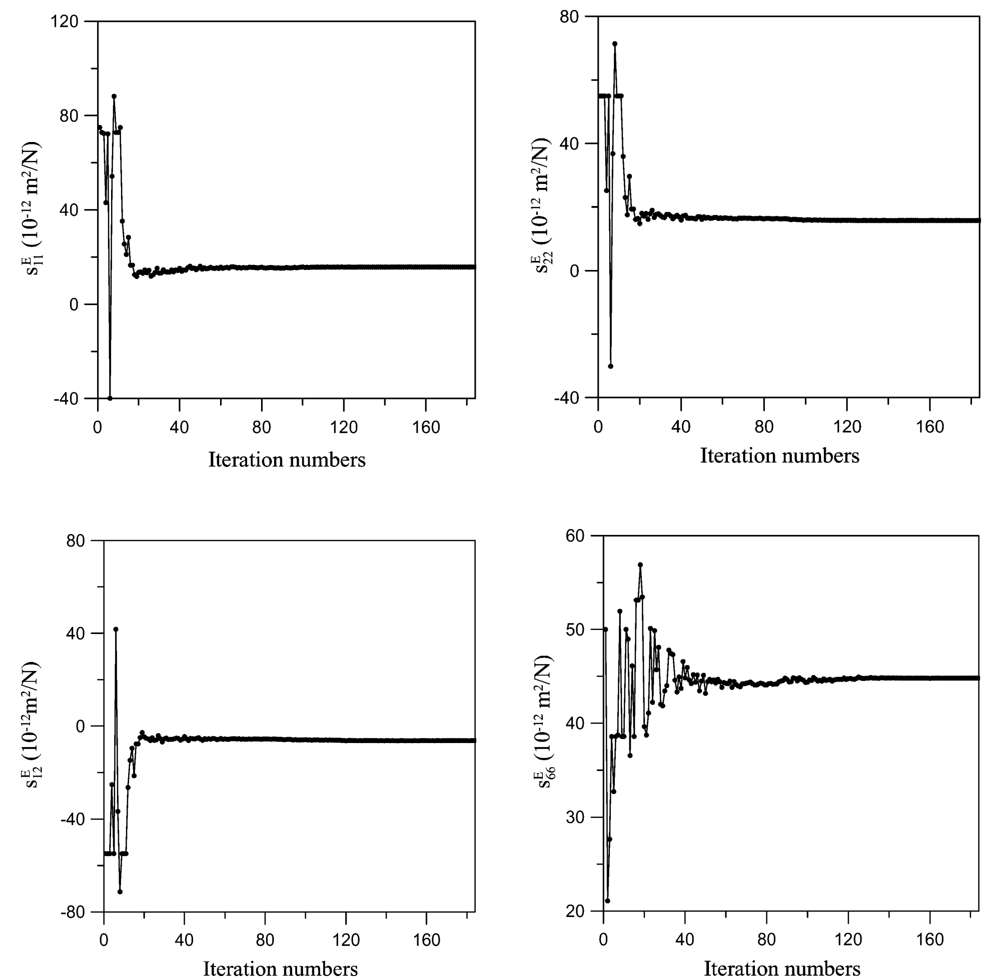

Fig. 3 Iteration and convergence of material compliance constants for fifth initial guess of piezoceramic rectangular plate.

According to the IEEE Standard on Piezoelectricity,[17] the compliance constants s_{11}^E and s_{12}^E can be determined by the radial in-plane (extensional) modes of a circular disk. Under the assumption that the electrical admittance will approach infinity at resonant frequencies, the characteristic equation for resonant frequencies with free-circumferential boundary conditions can be expressed summarily as follows:

$$\eta_n J_0(\eta_n) = (1 - \sigma^p) J_1(\eta_n) \tag{23}$$

and the resonant frequencies can be expressed as

$$f_n = (\eta_n / 2\pi a)\sqrt{1\Big/\left\{\rho s_{11}^E[1 - (\sigma^p)^2]\right\}} \tag{24}$$

where a is the radius of the disk and $\sigma^p = -s_{12}^E / s_{11}^E$ is the planar Poisson's ratio. The ratio of the first overtone to the fundamental resonant frequencies ($f_s^{(2)}/f_s$) depends only on σ^p and can be given as a function of σ^p in tabular form.[17] In this way, the planar

Table 5 Resonant frequencies of radial in-plane modes obtained by AF-EPSI, impedance analysis, FEM, and Eq. (24)

Radial in-plane mode	AF-ESPI, Hz	Impedance analysis, Hz	FEM, Hz	Eq. (24), Hz
1	68,400	69,065	64,389	64,396
2	178,940	179,010	167,698	167,786

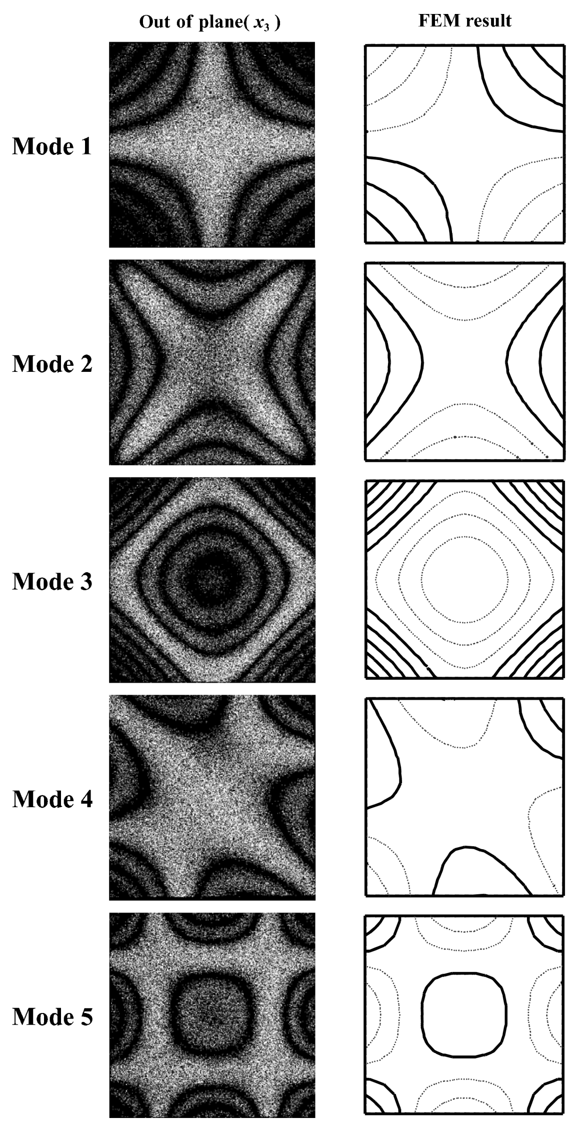

Fig. 4 First five out-of-plane mode shapes obtained by AF-ESPI and FEM.

Poisson's ratio σ^p can be found, and, subsequently, s_{11}^E can be calculated from Eq. (23). Herein we also employ a PIC-151 piezoceramic disk (diameter = 30 mm and thickness = 0.5 mm) to perform the method and compare the results with those mentioned earlier. Table 5 shows the resonant frequencies of radial in-plane modes obtained by AF-ESPI, impedance analysis, the FEM, and Eq. (24). The numerical calculations by the FEM and Eq. (24) are both carried out using the theoretical material constants. The inverse evaluation results by radial in-plane modes according to AF-ESPI measurement are shown in Table 6. When the difference in Table 3 is compared with that in Table 6, the Rayleigh–Ritz method incorporated with the Simplex algorithms is sufficient to develop the inverse evaluation methodology. Note that the vibration modes used for the Rayleigh–Ritz method are out-of-plane (transverse) types and those used for the IEEE Standard are in-plane (extensional) types. Both of these vibration types can be measured by the AF-ESPI method, which has been discussed earlier. Figure 5 shows the radial in-plane mode shapes for a piezoceramic disk by AF-ESPI and Fig. 6 is the corresponding impedance variation curve. The local minima appearing in the impedance variation curve correspond to resonant frequencies. Note that only the resonant frequencies of the radial in-plane modes are indicated in Fig. 6, that is, those of the out-of-plane modes cannot be obtained by impedance analysis.

Table 6 Comparison of inverse evaluations with theoretical values by radial in-plane modes

Compliance constants	s_{11}^E, $10^{-12}\mathrm{m}^2/\mathrm{N}$	s_{22}^E, $10^{-12}\mathrm{m}^2/\mathrm{N}$	s_{12}^E, $10^{-12}\mathrm{m}^2/\mathrm{N}$	s_{66}^E, $10^{-12}\mathrm{m}^2/\mathrm{N}$
Inverse evaluation	14.62	14.62	−4.692	38.624
Theoretical value	16.83	16.83	−5.656	44.97
Difference, %	13.13	13.13	17.04	14.11

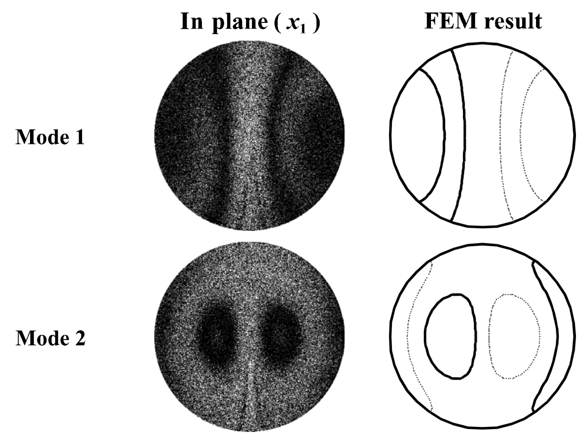

Fig. 5 First two radial in-plane mode shapes obtained by AF-ESPI and FEM.

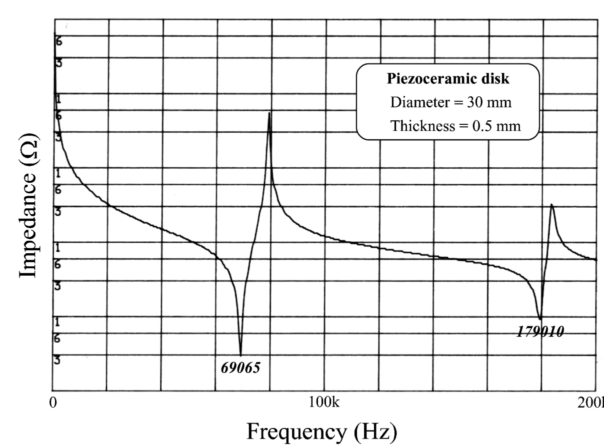

Fig. 6 Impedance variation curve of piezoceramic disk.

Conclusions

Optical techniques have been recognized with certain advantages for dynamic analysis, and ESPI has been used for many types of vibration measurement. In this paper, a self-arranged AF-ESPI optical setup with good visibility and noise reduction has been established to obtain experimentally both the resonant frequencies and the corresponding mode shapes of piezoceramic plates. A computer program is used in which equations derived by the Rayleigh–Ritz method are developed to determine the resonant frequencies for traction-free piezoceramic rectangular plates of out-of-plane vibrations. The Simplex iteration algorithms are incorporated within the computer program for the inverse evaluation of compliance constants that dominate the out-of-plane vibration characteristics. The difference between the inverse calculated results and the theoretical values is below 10% and is mainly due to the errors induced by measuring the resonant frequencies from the AF-ESPI technique, the accuracy of the Rayleigh–Ritz method, and the suitability of application for the orhotropic plate theory. When compared with the IEEE Standard[17] method using radial resonant frequencies, the inverse evaluation methodology utilizing the out-of-plane vibration modes of much lower resonant frequencies could provide another strategy to determine the material constants.

Acknowledgment

The author gratefully acknowledges financial support of this research by the National Science Council (Taiwan, Republic of China) under Grant NSC 90-2212-E-231-003.

References

[1]Butters, J. N., and Leendertz, J. A., "Speckle Pattern and Holographic Techniques in Engineering Metrology," *Optics and Laser Technology*, Vol. 3, No. 1, 1971, pp. 26–30.

[2]Rastogi, P. K., *Holographic Interferometry*, Springer-Verlag, Berlin, 1994, Chap. 2.

[3]Jones, R., and Wykes, C., *Holographic and Speckle Interferometry*. Cambridge Univ. Press, Cambridge, England, U.K., 1989, Chap. 4.

[4]Lϕkberg, O. J., and Hogmoen, K., "Use of Modulated Reference Wave in Electronic Speckle Pattern Interferometry," *Journal of Physics E: Scientific Instruments*, Vol. 9, No. 10, 1976, pp. 847–851.

[5]Shellabear, M. C., and Tyrer, J. R., "Application of ESPI to Three-Dimensional Vibration Measurements," *Optics and Lasers in Engineering*, Vol. 15, No. 1, 1991, pp. 43–56.

[6]Lϕkberg, O. J., "Mapping of In-Plane Vibration Modes by Electronic Speckle Pattern Interferometry," *Optical Engineering*, Vol. 24, No. 2, 1985, pp. 356–359.

[7]Doval, A. F., Fernández, J. L., Pérez-Amor, M. J., Valera, D. R., and Jones, J. D. C., "Contrast Enhanced and Phase Controlled Stroboscopic Additive Fiber Optic TV-Holography for Whole Field Out-of-Plane Vibration Analysis," *Optics and Lasers in Engineering*, Vol. 25, No. 4-5, 1996, pp. 323–342.

[8]Pouet, B., Chatters, T., and Krishnaswamy, S., "Synchronized Reference Updating Technique for Electronic Speckle Interferometry," *Journal of Nondestructive Evaluation*, Vol. 12, No. 2, 1993, pp. 133–138.

[9]Wang, W. C., Hwang, C. H., and Lin, S. Y., "Vibration Measurement by the Time-Averaged Electronic Speckle Pattern Interferometry," *Applied Optics*, Vol. 35, No. 22, 1996, pp. 4502–4509.

[10]Ma, C. C., and Huang, C. H., "The Investigation of Three-Dimensional Vibration for Piezoelectric Rectangular Parallelepipeds Using the AF-ESPI Method," *IEEE Transactions on Ultrasonics, Ferroelectrics, and Frequency Control*, Vol. 48, No. 1, 2001, pp. 1–12.

[11]Huang, C. H., and Ma, C. C., "Vibration Characteristics for Piezoelectric Cylinders Using Amplitude-Fluctuation Electronic Speckle Pattern Interferometry," *AIAA Journal*, Vol. 36, No. 12, 1998, pp. 2262–2268.

[12]Berlincourt, D. A., Curran, D. R., and Jaffe, H., "Piezoelectric and Piezomagnetic Materials and Their Function in Transducers," *Physical Acoustics*, Vol. 1, Pt. A, Academic Press, New York, 1964, pp. 169–270.

[13]Zelenka, J., *Piezoelectric Resonators and Their Application*, Academia, Prague, 1986, Chap. 6.

[14]Tiersten, H. F., *Linear Piezoelectric Plate Vibration*, Plenum, New York, 1969, pp. 33–61.

[15]Bechmann, R., "Elastic, Piezoelectric, and Dielectric Constants of Polarized Barium Titanate Ceramics and Some Applications of the Piezoelectric Equations," *Journal of the Acoustical Society of America*, Vol. 28, No. 2, 1956, pp. 347–350.

[16]Meitzler, A. H., O'Bryan, H. M., Jr., and Tiersten, H. F., "Definition and Measurement of Radial Mode Coupling Factors in Piezoelectric Ceramic Materials with Large Variations in Poisson's Ratio," *IEEE Transactions on Sonics and Ultrasonics*, Vol. su-20, No. 3, 1973, pp. 233–239.

[17]"IEEE Standard on Piezoelectricity," Standard 176-1987, American National Standards Inst./Inst. of Electrical and Electronics Engineerings, New York, Jan. 1988.

[18]Chang, S. H., Rogacheva, N. N., and Chou, C. C., "Analysis of Methods for Determining Electromechanical Coupling Coefficients of Piezoelectric Elements," *IEEE Transactions on Ultrasonics, Ferroelectrics, and Frequency Control*, Vol. 42, No. 4, 1995, pp. 630–640.

[19]Kosinski, J. A., Ballato, A., and Lu, Y., "A Finite Plate Technique for the Determination of Piezoelectric Material Constants," *IEEE Transactions on Ultrasonics, Ferroelectrics, and Frequency Control*, Vol. 43, No. 2, 1996, pp. 280–284.

[20]Young, D., "Vibration of Rectangular Plates by the Ritz Method," *Journal of Applied Mechanics*, Vol. 17, No. 4, 1950, pp. 448–453.

[21]Ambartsumyan, S. A., *Theory of Anisotropic Plates: Strength, Stability, and Vibrations*, Hemisphere, New York, 1991, Chap. 2.

[22]Ma, C. C., and Lin, C. C., "Inverse Evaluation of Material Constants for Composite Plates by Optical Interferometry Method," *AIAA Journal*, Vol. 37, No. 8, 1999, pp. 947–953.

[23]Hibbit, H. D., Karlsson, B. J., and Sorensen, A., *ABAQUS User's Manual*, Ver. 5.5, Hibbit, Karlsson, and Sorensen, Inc., Pawtucket, RI, 1995.

C. Pierre
Associate Editor